

Local distribution approach to disordered systems

A. Alvermann and H. Fehske

Ernst-Moritz-Arndt-Universität Greifswald, Germany

(Dated: December 2, 2024)

We discuss an approach to disordered systems which is based on a selfconsistent scheme for the distribution of local Green functions. The applicability of this approach is discussed, and exemplarily demonstrated for the Anderson model of localization, the binary alloy and percolation model. The importance to consider distributions is underlined by a comparison to theories based on selfconsistent schemes for averaged Green functions, whose shortcomings are discussed.

Keywords: Disordered systems, Anderson localization, binary alloy, quantum percolation.

I. MOTIVATION AND INTRODUCTION

To tackle the major problem of interacting disordered systems a sufficiently simple but rather complete theory for the disorder problem has to be developed as the cornerstone for a general theory which should incorporate all the subtle effects beyond diffusive motion being at the focus since the advent of localization theory.¹ Elaborate numerical approaches to the localization problem, e.g. the transfer matrix method (TMM)², which keep explicitly track of non-local correlations, have a high computational complexity. Combining these methods with a reliable description of particle interactions would demand computational resources far beyond everything available in the nearby future.

This severe limitation has renewed the interest in simple schemes which map the disordered system onto the simpler problem of a local impurity in an averaged medium, similar in spirit though different in construction to the dynamical mean field theory (DMFT)³ approach to interacting systems. The most well known example of these is the coherent potential approximation (CPA).⁴ Various studies of Anderson and disordered Hubbard models, based on CPA or its variants, have been carried out recently.^{5,6,7,8}

Disorder effects are retained in these averaging theories only through renormalization of certain parameters, e.g. by introducing an effective bandstructure or a finite mean free path. Although some general features of disordered systems certainly can be reproduced, e.g. damping or diffusion, the more subtle effects as Anderson localization or band fragmentation in the binary alloy are beyond their scope. To overcome these shortcomings cluster extensions of the CPA scheme have been worked out.⁹ Such cluster extensions reintroduce non-local correlations partially. However, a fully convincing description has not yet been obtained in such a way.

But already 30 years ago a different scheme has been proposed by Abou-Chacra, Anderson, and Thouless¹⁰ ('AAT' for short), which is both based on a local description, and satisfactorily complete. The main point they made is not to look on averages but on distributions of local quantities. Non-local correlations which are important for a proper description of localization are not explicitly calculated, but implicitly contained in the

distribution.

The success of AAT, which will become apparent in explicit calculations, can be understood by two arguments. First, in any real disordered medium the moving particles strongly feel the difference in potential energy in the vicinity of an impurity or far away from it. Hence the particle motion changes from homogenous Bloch waves to a motion which depends on the particle position with respect to the impurity. The spatial fluctuations in the particle motion are neglected if a simple effective medium replaces the disordered system. This effect is present for a single impurity, and does not average out for many impurities (if it did we would end up with purely diffusive motion). All averaging theories suffer from this neglection. To overcome it, the spatial fluctuations of particle motion, i.e. their distribution, must be incorporated in the theory. Second, Anderson localization takes place on large length scales: in any finite system localization is, strictly speaking, absent. But the mechanism which leads to localization, i.e. impurity scattering, is of a local kind. A large amount of localization physics is thus dominated by local behavior and can be obtained within a local approach, as long as non-local correlations are at least implicitly accounted for, e.g. by using distributions. Exceptions to this are the critical behaviour close to the transition, and weak localization in the critical dimension $d = 2$.

AAT benefits from these two insights: we must respect the statistical character, but we can adopt a local point of view. In this article we are going to demonstrate that the AAT scheme gives a surprisingly comprehensive and detailed description of the problem at hand. Since AAT has only moderate computational demands, compared to nowadays accessible resources, detailed calculations can be performed which had not been possible at the time of its derivation.

II. MODEL AND DISTRIBUTIONS

Our study of disorder phenomena deals with the model

$$H = \sum_i \epsilon_i |i\rangle\langle i| - t \sum_{\langle ij \rangle} |i\rangle\langle j| + |j\rangle\langle i| \quad (1)$$

which describes a tight-binding electron on a lattice with site-diagonal disorder ϵ_i (t is chosen to give a full bandwidth $W = 1$, so we measure disorder in units of W). The distribution of ϵ_i , which are assumed to be identically independently distributed random variables, determines the specific type of model. Three cases will be discussed in this article's main part: the Anderson model, the binary alloy model, and the (quantum) percolation model. We shall be neither concerned with 'bond' disorder in the hopping matrix element t nor with correlations between the ϵ_i , although both cases can be treated within the AAT scheme.

For a given realization of the random variables ϵ_i the local density of states (LDOS) $\rho_i(\omega) = -\text{Im } G_{ii}(\omega + i\eta)/\pi$ has a definite value on each lattice site i . If we consider all realizations of ϵ_i for fixed disorder distribution, the local density of states is a random variable in its own right, with a certain probability distribution $p(\rho_i, \omega, \eta)$. According to the model assumptions $p(\rho_i, \omega, \eta)$ does not depend on the lattice site i . By definition it is self-averaging, and the distribution on one lattice site for all realizations of the ϵ_i is identical to the distribution on all lattice sites for one 'typical' realization of the ϵ_i . A basic physical quantity that is calculated from $p(\rho_i, \omega, \eta)$ is the *arithmetically averaged density of states* (averaged DOS)

$$\rho_{\text{ave}}(\omega) := \lim_{\eta \rightarrow 0} \int_0^\infty \rho_i p(\rho_i, \omega, \eta) d\rho_i \quad (2)$$

which counts the number of states at energy ω .

Localized and extended states reflect itself in different spectral properties of the Hamiltonian. While extended states ('scattering states') come along with an absolutely continuous spectrum, localized states correspond to a pure point spectrum. The intriguing feature of disordered systems is the possibility of a dense pure point spectrum. This possibility is responsible for many of the difficulties encountered in the study of Anderson localization if compared to the case of single impurities where only isolated poles can exist. The information about the spectrum is contained in the distribution $p(\rho_i, \omega, \eta)$, but is lost in the averaged quantity $\rho_{\text{ave}}(\omega)$. To understand how the information about localization can be extracted from $p(\rho_i, \omega, \eta)$ let us consider the two quantities $I_1(\omega) := \lim_{\eta \rightarrow 0} \int_0^\infty p(\rho_i, \omega, \eta) d\rho_i$ and

$$I_2(\omega) := \lim_{\xi \rightarrow \infty} \lim_{\eta \rightarrow 0} \int_0^\xi p(\rho_i, \omega, \eta) d\rho_i. \quad \text{Independent of its}$$

structure any eigenstate of the Hamiltonian contributes an η -broadened Lorentzian to $\rho_i(\omega)$ hence the normalization condition $I_1(\omega) = 1$ is fulfilled. But localized states which corresponds to a point spectrum will not contribute to $p(\rho_i, \omega, \eta)$ for $\eta \rightarrow 0$. So, if localized states exist at energy ω , $I_2(\omega) < 1$. While $I_2(\omega) = 0$ implies that all states are localized, $0 < I_2(\omega) < 1$ would imply coexistence of localized and extended states. In fact $I_2(\omega)$ gives the fraction of extended states at ω .

Unfortunately I_2 is difficult to evaluate in course of the order of limits in its definition. One simple choice which can partially replace I_2 in the case of the Anderson model is the *geometrically averaged density of states*

$$\rho_{\text{geo}}(\omega) = \lim_{\eta \rightarrow 0} \exp \left(\int_0^\infty \ln p(\rho_i, \omega, \eta) d\rho_i \right). \quad (3)$$

One can convince oneself by analyzing the $\eta \rightarrow 0$ scaling, that $I_2 \rightarrow 0$ while $I_1 = 1$ implies $\rho_{\text{geo}} = 0$, and vice versa. So ρ_{geo} acts as substitute for I_2 , fitting the technical demands met in a numerical calculation.

It is important to realize that a finite value of $\rho_{\text{geo}}(\omega)$ has no direct physical meaning. Let us stress this point: $\rho_{\text{geo}}(\omega)$ does *not* count the number of localized states. Moreover it is no true order parameter for the localization problem, and there is no reason to elaborate on its critical behavior.

III. AAT SCHEME

The AAT scheme is most conveniently constructed on a Bethe lattice (coordination number K , $K = 2$ if not stated otherwise) where the local Green function

$$G_{ii}(\omega + i\eta) = \left[\omega + i\eta - \epsilon_i - t^2 \sum_{j=1}^K G_{jj}(\omega + i\eta) \right]^{-1} \quad (4)$$

can be expressed through its value on the neighboring lattice sites $j = 1, \dots, K$. Due to the special geometry of the Bethe lattice this equation can be interpreted as a self-consistency equation for the distribution of $G_{ii}(\omega)$.^{10,11} Be aware that then the indizes i, j do not denote specific lattice sites but certain realizations of the random variable $G_{ii}(\omega)$. For the ordered system (all $\epsilon_i = 0$) this equation simplifies to the well-known recursion relation ('renormalized perturbation expansion') for the Green function $G^0(\omega) = (8/W^2)(\omega - \sqrt{\omega^2 - W^2/4})$ of the Bethe lattice,¹² with bandwidth $W = 4t\sqrt{K}$. For $K = \infty$, taking into account the scaling $t \propto 1/\sqrt{K}$ of the hopping matrix element, the sum over j in Eq. (4) can—assuming the central limit theorem to be applicable—be replaced by the arithmetic average of G_{jj} , and the CPA is recovered. Conversely, AAT can be understood as an infinite cluster extension of CPA. For a disordered system in $K < \infty$ the solution of Eq. (4) is obtained through a Monte-Carlo procedure (Gibbs sampling). The distribution is represented through a sample of typically 5×10^4 up to 2.5×10^7 elements, depending on the respective case studied. At each step of iteration a new sample is constructed whose elements are calculated through Eq. (4) with a randomly chosen ϵ_i and K elements drawn from the previous sample. A hundred up to some thousand iterations are necessary to guarantee convergence.¹¹ In course of its construction AAT works on an infinite

lattice (no boundaries, no finite size effects, no finite energy resolution). The size of the sample determines the resolution which the distribution is sampled with. The maximal resolution can be easily enhanced by increasing the sample size (see below).

Let us remark on one important point: The choice of the Bethe lattice is no real drawback for the study of localization as advocated for in this article. As pointed out in the introduction the interference effect leading to (exponential) localization stems from local scattering, hence is included in AAT. But AAT cannot help to calculate e.g. critical exponents for the cubic lattice since the critical behaviour on the Bethe lattice is different from the hypercubic case.¹³ This can be attributed to the geometrical structure of the Bethe lattice (number of sites grows exponentially with distance), which is part of the large scale structure of the studied problem. For our purposes this restriction is mild. In a real system where physics is dominated by complicated interdependencies of disorder and interaction, universality classes may play not the only role. A major role can be attributed to cooperative effects, e.g. formation of polaronic defect states, which come along with highly non universal behaviour.¹¹

IV. ANDERSON MODEL

The Anderson model—which is the prototype model showing a localization transition—is obtained for a uniform distribution of ϵ_i in the interval $[-\gamma/2, \gamma/2]$,

$$p(\epsilon_i) = \frac{1}{\gamma} \Theta\left(\frac{\gamma}{2} - |\epsilon_i|\right) . \quad (5)$$

The characteristics of localization show up in $p(\rho_i, \omega, \eta)$ (cf. Fig. (1)). Impurity scattering causes the distribution to be strongly asymmetric and broad even for extended states. As one consequence the averaged density of states is on a different scale than the ‘typical’ value. On approaching the localization transition the asymmetry further increases. Much weight is transferred to large values of ρ_i , while the ‘typical’ value tends to zero.

A closer look on the distributions reveals that near the localization transition the distribution shows a perfect power law behaviour over a wide range of ρ_i . Its exponent is $\simeq 1.45$, which is reasonably close to the analytical results obtained from field theoretical considerations.^{13,14,15}

Passing the localization transition the distribution becomes singular, corresponding to a transition from continuous to discrete spectrum, i.e. from $I_2 = 1$ to $I_2 = 0$. This characteristic change reflects itself most clearly in the dependence of the distribution on the η -regularization. While the distribution for extended states is stable under decreasing η , the scale of the distribution for localized states is entirely set through η . This distribution will become singular for $\eta \rightarrow 0$ in accordance with our general considerations before. To use this different behaviour as a localization criterion amounts to perform

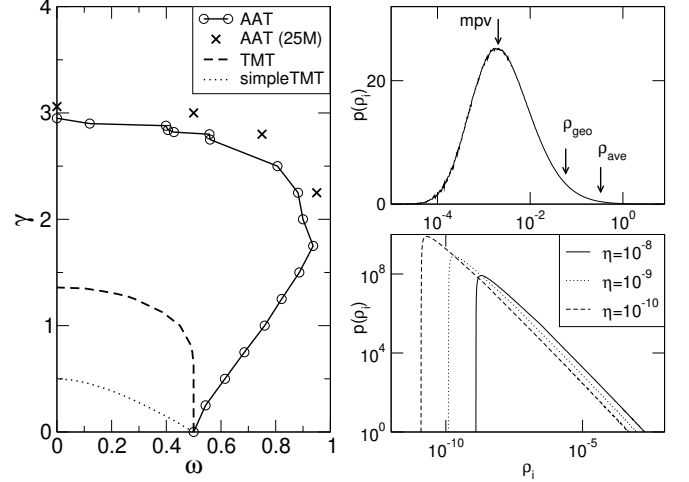


FIG. 1: Left: Phase diagram of the Anderson model. The solid (dashed, dotted) curve shows the mobility edge trajectory calculated within AAT (TMT, simplified TMT) by means of the $\eta \rightarrow 0$ limit, using a sample with 5×10^4 elements. The crosses indicate points in the (ω, γ) -plane corresponding to the mobility edge position for an extremely large sample of 2.5×10^7 elements. Right top: probability distribution of LDOS for extended states, at $\gamma = 1.5$, $\omega = 0.0$. The distribution is – for not too large values of η – independent of η . Right bottom: probability distribution of LDOS for localized states, at $\gamma = 1.5$, $\omega = 0.9$, and three values of η .

the $\eta \rightarrow 0$ limit numerically. In practice one tracks the decay of ρ_{geo} as $\eta \rightarrow 0$. Precisely if ρ_{ave} stays finite while $\rho_{\text{geo}} \rightarrow 0$ with $\eta \rightarrow 0$ a localized state is detected. This criterion does not depend on any a priori choice or approximation, hence should be considered ‘numerically exact’.

The AAT phase diagram for the Anderson model which has been obtained by performing the $\eta \rightarrow 0$ -limit in the (ω, γ) -plane shows the characteristic features for the localization problem in three dimensions.^{16,17} In the simplest picture available localization is governed by the interplay of two competing effects. First, tunneling between shallow impurities produces, for small disorder, extended states outside the bare tight-binding band. Second, strong scattering on deep impurities takes place with increasing disorder, starting to localize formerly extended states. So the mobility edge trajectory shows a reentrant behaviour and the existence of a critical disorder $\gamma_c \approx 2.9$ for complete localization.

As an additional effect coherent (back-)scattering causes quantum interference on closed loops. This effect is not accessible on the Bethe lattice where all loops have been discarded. As we have already mentioned in the introduction the corresponding phenomena of weak localization is beyond an AAT description. Fortunately it is not an important ingredient in the situations which are in our primary focus. Indeed we expect weak localization to be masked by exponential localization in any dimension but $d = 2$.

We already mentioned that the finite size of the Monte-Carlo sample sets the resolution for sampling $p(\rho_i, \omega, \eta)$. In the strong scattering regime, but still for extended states, $p(\rho_i, \omega, \eta)$ is concentrated at small values of ρ_i . If the sample (and thus the resolution) is too small the distribution will be falsely detected as singular while a larger sample correctly gives a regular distribution corresponding to extended states. So if the sample size is increased the mobility edge is shifted to larger values of disorder. The points on the mobility edge trajectory stabilize if the sample is chosen large enough. Although a priori errors cannot be established—the same is true for almost any numerical method, e.g. the transfer matrix method (TMM)—increasing the sample size allows for an arbitrarily precise determination of the mobility edges.

In contrast to AAT the CPA fails to detect localization of states. Thinking in distributions this is roughly attributed to the fact that the averaged density of states is no good ‘estimator’ for the broad distribution close to the localization transition. In line with this attribution the typical medium theory (TMT)⁵ modifies the CPA self-consistency condition with $\rho_{\text{ave}}(\omega)$ replaced by $\rho_{\text{geo}}(\omega)$ (which nevertheless does not approximate the ‘typical’ values, cf. Fig. 1). If we compare the lines of vanishing $\rho_{\text{geo}}(\omega)$ from TMT (i.e. the ‘TMT mobility edges’) with the AAT phase diagram we see the consequences of this modification. The critical disorder predicted is far too small to be attributed to a localization transition caused by scattering and interference. The reader should be aware that the correct critical disorder increases with dimension thus is always large compared to the TMT prediction. Furthermore the reentrant behaviour of the mobility edge is entirely missed.

These shortcomings result from the TMT construction. Replacing the averaged by the geometric density of states leads to an overestimation of the scattering on deep impurities. Of course the density of states is reduced, but the effect is exactly the one obtained for a single impurity where states are pushed outside the band. Adding up these scattering events finally sets the density of states to zero, mimicking a localization transition. The reentrant behaviour is missed since the impurity states that hybridize are completely removed from the theory. But a reduction of the number of states counted and a change in the nature of eigenstates is quite a different matter. TMT gives no description of interference and localization but of a damping effect caused by overestimated impurity scattering.

In fact TMT can be further simplified, replacing $\rho_{\text{geo}}(\omega)$ by $\min\{\rho_i(\epsilon_i = \gamma/2), \rho_i(\epsilon_i = -\gamma/2)\}$. This ‘averaging procedure’ drastically overestimates the strength of impurity scattering, and the ‘simplified TMT’ is surely far away from any reasonable description of the underlying physics. However, the phase diagram obtained is very similar to the TMT one. Of course the critical disorder has to be even smaller than in TMT.

So much the worse, TMT is based on a misconception: $\rho_{\text{geo}}(\omega)$ enters the TMT equation (relating the

bath Green function to the local impurity one) in the same sense as $\rho_{\text{ave}}(\omega)$ does in CPA. The distribution of the local density of states in TMT is determined by the Lorentzian form $1/(\omega - \epsilon - t^2 \sum G)$ which is different from the approximate log-normal distribution that the geometrical density of states has been presumably designed for. Therefore the geometrical density of states has lost its meaning inside TMT. Its only effect is to reduce the density of states strongly even for weak disorder, and finally push it to zero. One is urged to conclude that it sets up a selfconsistency equation with the wrong solution properties which appear to describe Anderson localization only at a first glance. Besides the physical shortcomings already present for the noninteracting disordered system TMT has some technical inconsistencies, e.g. violation of sum rules, which renders a combination with interaction at least doubtful.

V. BINARY ALLOY MODEL

In contrast to the Anderson model with a ‘smooth’ impurity distribution the binary alloy model assumes a bimodal distribution

$$\rho(\epsilon_i) = c_A \delta(\epsilon_i - E_A) + (1 - c_A) \delta(\epsilon_i - E_B) . \quad (6)$$

We set $E_A = -\Delta/2$, $E_B = \Delta/2$, with $\Delta = E_B - E_A$. The complicated physics of the binary alloy model has been reported on previously.^{18,19} However, studies of the binary alloy model with interaction are so far based on a CPA treatment of disorder, or simplified variants thereof.^{6,7} A successful application of AAT to the binary alloy model would allow for a better understanding of the important physical questions behind these studies.

A. Low A-concentration – small separation energy

Let us first study the situation of low concentration $c_A = 0.1$ of A-atoms (which is below the classical percolation threshold, cf. Sec. VII). The A-atoms can be considered as the minority species in a bulk system of B-atoms (doping a semiconductor is an example).

For small separation energy $\Delta = 0.3$ the energy levels of the minority A-atoms lie inside the B-bulk-band. The averaged density of states mainly consists of the broad B-band centered at $E_B = +0.15$, but shows some additional structures at the lower band edge, which are absent in the CPA density of states (cf. Fig. 2). They originate from the strong fluctuations in the local environment of an atom, and can be best seen in the distribution of the local density of states (cf. Fig. 3). In contrast to the Anderson model it is multipeaked.

To understand the origin of the various peaks we define the ‘conditional’ local density of states $\rho_i^{A/B}(\omega)$, subject to the constraint that an A- respectively B-atom is located at site i . More generally we can specify a certain

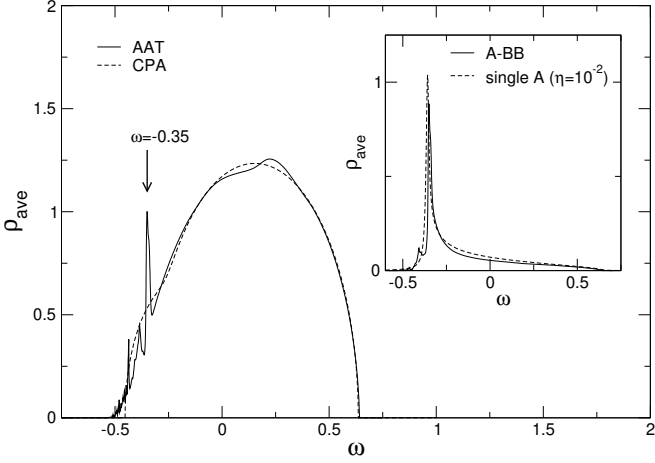


FIG. 2: Averaged density of states for the binary alloy with $E_A = -0.15$, $E_B = 0.15$, $c_A = 0.1$. The dashed curve shows the CPA result. The inset displays the conditional averaged DOS for the cluster configuration $A - BB$, the dashed curve has been calculated using Eq. (7) with broadening $\eta = 10^{-2}$ (see text).

atom configuration on a cluster of sites centered at i . Similarly other ‘conditional’ quantities are defined. By considering larger and larger clusters every peak in the distribution (and density of states) can be attributed to a specific configuration (cf. Fig. 3). As the simplest example the pronounced peak at $\omega \approx -0.35$ results from a single A-atom surrounded by B-atoms (cf. inset Fig. 2). Its position and form approximately follow from the simple formula

$$G_A(\omega) = \left[\frac{\omega + E_B}{2} - E_A + \sqrt{\left(\frac{\omega - E_B}{2} \right)^2 - \frac{W^2}{16}} \right]^{-1} \quad (7)$$

for the local Green function of one A-impurity embedded in a B-lattice. The corresponding density of states, with a broadening of $\eta = 0.02$ to mimic the effects of hybridization, fits the conditional averaged DOS very well (dashed curve in inset of Fig. 2). The complementary situation of a B-atom surrounded by A-atoms contributes to the ‘hump’ in the B-band (cf. Fig. 2), which arises from B-atoms neighboring to A-atoms.

It should be noted that Eq. (7) gives a δ -peak outside the B-band, corresponding to the impurity state at the A-atom, only above a critical value of Δ . This is another evidence that the Bethe lattice can be understood as an approximation to lattices in dimensions $d \geq 3$.

B. Low A-concentration – split band case

Increasing the separation energy to $\Delta = 2.0$ (still with $c_A = 0.1$) leads to the split band case (see Fig. 4). The

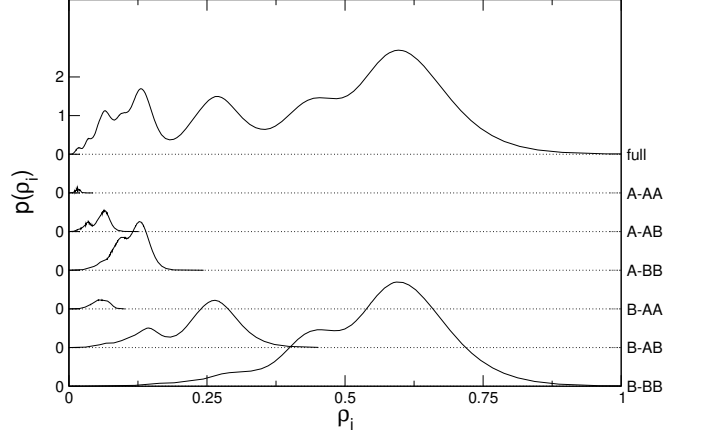


FIG. 3: Distribution of the LDOS for the binary alloy with parameters as in Fig. 2, at $\omega = 0.6$ (curve on top). The six other curves show the distribution of the conditional LDOS for a specified cluster of three sites.

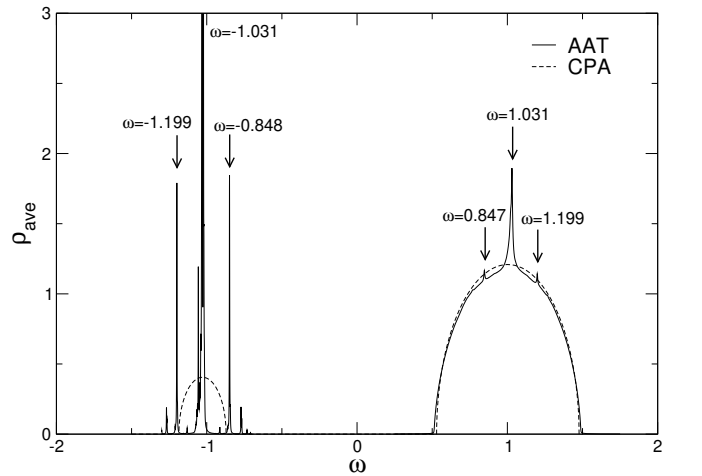


FIG. 4: Averaged DOS for the binary alloy with $E_A = -1.0$, $E_B = 1.0$, $c_A = 0.1$, with broadening $\eta = 10^{-3}$. Arrows mark the position of three peaks each in the A- and B-band.

majority B-atoms still form a band whose averaged density of states shows some additional spikes. The minority A-atoms form a fragmented set of peaks with varying height and width. Again these peaks emerge from A-clusters embedded in the B-lattice. The central peak at $\omega = -1.031$ whose position can be again calculated with Eq. (7) corresponds to a single A-atom surrounded by B-atoms. Similarly the two side peaks result from two adjacent A-atoms, and so forth. The weight of these peaks decreases exponentially as c_A^N for a N -atomic cluster. The complementary configurations, reversing the role of A- and B-atoms, yield spikes in the B-band. Since the concentration of B-atoms is large these spikes do not form peaks but merge with the B-band.

The concentration of A-atoms is below the classical percolation threshold hence only finite A-clusters exist. Due to the large separation energy the ‘A-states’ on these

clusters are strongly damped through scattering on B-atoms. Accordingly the ‘A-states’ do not hybridize to a band of conducting states. Thus we expect that all ‘A-states’ are localized, while the ‘B-band’ remains extended. Indeed if we track $p(\rho_i, \omega, \eta)$ for $\eta \rightarrow 0$ we find it to be singular in the energy range of the ‘A-states’ but regular for the B-band. Note that even for the multi-peaked distributions in the binary alloy the principle considerations from the introduction give valuable results.

If we compare the AAT data to the CPA we observe the breakdown of the latter one. The CPA is unable to capture the fragmentation of the spectrum. As we have already discussed this failure can be attributed to the neglection of spatial fluctuations. Let us briefly remark that in this case TMT produces curious results which do not correspond to any physically sensible behaviour. Of course this could be expected from the structure of $p(\rho_i, \omega, \eta)$ in the binary alloy (see Fig. 3), which renders a mapping on an effective averaged medium impossible.

C. Equal A/B-concentration

So far we have dealt with a low concentration c_A of the A-species below the classical percolation threshold. Then, when only finite A-clusters exist, strong signatures and fragmentation of the density of states could be observed. For equal concentration $c_A = c_B = 0.5$, which corresponds not to a doped material but to a stoichiometric compound, these signatures should be reduced, but still exist (cf. Fig. 5). Since for $K = 2$, with percolation threshold $p_c = 1/K = 0.5$ (cf. Sec. VII), neither atom species is in the percolating regime—a peculiarity of the Bethe lattice—we calculated the averaged density of states here for $K = 3$.

While the CPA is unable to describe structures arising from spatial fluctuations we might expect it to perform better for a case where fluctuations should be of minor importance. But if we ask for the energy separation Δ at which the bands start to split CPA gives a value $\Delta = 1/2$ half as large as the expected one. From AAT we can get a much better picture (cf. Fig. 5). Remember that on increasing Δ the band starts to fragment so band splitting should be indeed observed below $\Delta = 1$. The failure of CPA has a similar reason as the failure of TMT on the critical disorder in the Anderson model. In both cases the damping due to scattering is overestimated by averaging the local Green function, whose full distribution only represents the correct physical behaviour.

VI. COMBINED ANDERSON AND BINARY ALLOY MODEL

The binary alloy model shows a very distinct behaviour that might be non-generic. To test this point we combine the binary alloy model with additional on-site box disorder γ (cf. Fig. 6). For the parameters considered

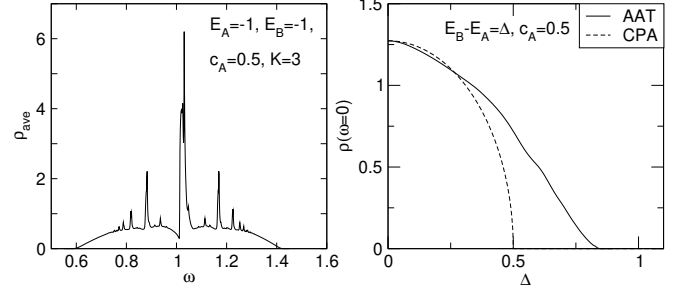


FIG. 5: Left: Split band case for equal concentration $c_A = c_B = 0.5$, in $K = 3$, with $\eta = 10^{-3}$. Right: Dependence of averaged DOS at energy $\omega = (E_A + E_B)/2 = 0$ on impurity energy separation $\Delta = E_B - E_A$.

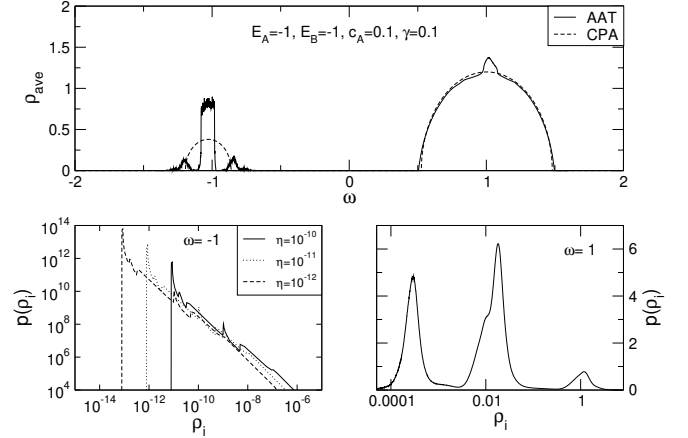


FIG. 6: Top: Averaged DOS in the split band case for low A-concentration, with additional on-site disorder for A- and B-atoms (box type as in Anderson model, parameter γ), with $\eta = 10^{-6}$. Bottom left: Distribution of LDOS in the center of the A-band at $\omega = -1$, for $\eta = 10^{-12}, 10^{-11}, 10^{-10}$ from left to right. Bottom right: Distribution of LDOS in the center of the B-band at $\omega = +1$, for $\eta = 10^{-30}$. The distribution is independent of η .

γ is on the same energy scale as the hopping matrix element $t = 1/\sqrt{32}$ (here tenth of full bandwidth, i.e. $\gamma \approx 0.56t$). The CPA density of states is the combination of two rescaled bands which otherwise resemble a ‘pure’ Anderson model. Again the CPA picture turns out to be too simple. As AAT shows the two bands have a complex internal structure with features similar to the ‘pure’ binary alloy. Evidently the system cannot be described in terms of rescaled Anderson models – a point which is (partially) missed in some studies.²⁰

It is reasonable to assume that in any real alloy, e.g. a doped semiconductor, the complex peaked structure of the binary alloy model will survive. Furthermore, having performed the $\eta \rightarrow 0$ -limit, we find the A-band to be entirely localized (cf. Fig. 6). Nevertheless γ is much smaller than the critical disorder $\gamma_c \approx 2.9$ for Anderson localization of the A-subband. Therefore localization of the A-band does not result from an Anderson type of

mechanism but from the strong scattering occurring for the minority band in the binary alloy. This suggest that impurity band states in a doped semiconductor will almost always be localized.

VII. QUANTUM PERCOLATION MODEL

In the extreme limit $E_B \rightarrow \infty$, keeping $E_A = 0$ fixed, the binary alloy model reduces to the percolation model where A-sites are embedded in an impenetrable host medium. Certainly, in a real alloy with $\Delta < \infty$, the electron has the chance to tunnel through the host barrier. Nevertheless, the percolation model shows general features in pure shape without the need to discuss additional hybridization arising from the tunneling process. Indeed the ‘percolation picture’ has already shown up in the split band case of the binary alloy model (see above).

Let us first study the averaged density of states. If the concentration c_A of A-atoms is below the classical percolation threshold p_c only finite clusters exist. The corresponding spectrum is a pure point spectrum which densely fills the energy intervall $[-W/2, W/2]$ of the bare tight-binding band (‘Dirac comb’). An N -site cluster with occurrence probability $c_A^N(1 - c_A)^{N+1}$ contributes peaks at energies spread over the full possible range. Consequently the weight of a peak varies in contrast to the Anderson model non-monotonically with ω . Different statistical properties of the finite clusters can be straightforwardly calculated on the Bethe lattice. For instance the weight

$$\begin{aligned} p_{\text{fin}} &= \sum_{N=1}^{\infty} c_A^{N-1}(1 - c_A)^{N+1} C_N \\ &= \begin{cases} 1, & c_A \leq 0.5 \\ (1 - c_A)^2/c_A^2, & c_A > 0.5 \end{cases} \end{aligned} \quad (8)$$

of all finite clusters (in $K = 2$) directly follows by help of the generating function for the Catalan numbers C_N , which give the number of binary trees with N sites. For concentrations above p_c ($= 0.5$), when $p_{\text{fin}} < 1$, an infinite percolating cluster exists. This clusters can support extended states which contribute to an continuous spectrum. Since the ‘effective’ dimension of the percolating cluster is smaller than K (especially close to p_c), the bandwidth of the resulting band is smaller than W .

The density of states shows strong signatures (peaks and dips), which are reminescent of the binary alloy (see top picture in Fig. 7). These signatures arise from both isolated finite clusters and finite clusters attached to the backbone of the infinite percolating cluster. With increasing concentration their weight reduces, and the signatures are washed out. At $\omega = 0$ a pronounced δ -peak surrounded by a dip in the density of states exists. With increasing concentration the peak reduces in weight and the dip narrows, eventually both merge to a spike in the band.

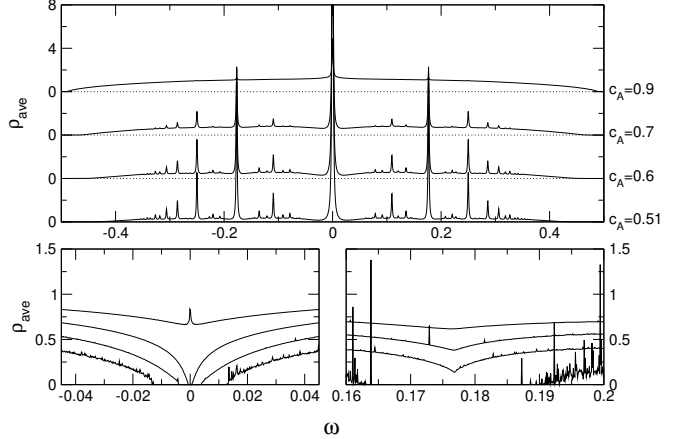


FIG. 7: Averaged density of states ρ_{ave} for the percolation model. Top picture: concentrations $c_A = 0.51, 0.6, 0.7, 0.9$ from bottom to top (broadening $\eta = 10^{-3}$). Bottom left: central region around $\omega = 0$ without Lorentzian broadening ($\eta = 10^{-20}$), for concentrations $c_A = 0.6, 0.65, 0.7, 0.75$ from bottom to top. Bottom right: region around the second peak at $\omega = t = 1/\sqrt{32} \approx 0.177$ without Lorentzian broadening ($\eta = 10^{-20}$), for concentrations $c_A = 0.55, 0.6, 0.65, 0.7$ from bottom to top.

The origin of this central peak and the dip can be understood on the same level of reasoning as for Eq. (7). If a single atom is attached to the backbone of the percolating cluster the Green function is modified by the additional hybridization from hopping to this atom. The hybridization is infinite at $\omega = 0$, which is the energy of the one atom eigenstate. The density of states thus shows a δ -peak at $\omega = 0$, which arises from the state located at the atom, and a dip around this peak which arises from the damping of states on the percolating cluster. The same argumentation holds for any finite cluster instead of a single atom. Since larger clusters have lower probability of occurrence the central peak is the most pronounced, and exists up to the largest concentrations.

Nevertheless the percolating cluster is not made up of its backbone plus one additional finite cluster, but many finite clusters attached to it. The Green function $G^c(\omega)$ of a (half-)infinite chain with one additional atom attached to *each* site obeys the recursion relation

$$G^c(\omega) = (\omega - t^2/\omega - t^2 K G^c(\omega))^{-1} \quad (9)$$

which is solved by $G^c(\omega) = G^0(\omega - t^2/\omega)$, where $G^0(\omega)$ is the Green function of the bare Bethe lattice. Of course $G^c(\omega = 0) = 0$ as before, but the diverging real part of $1/\omega$ produces not a dip but a *gap* in the density of states around $\omega = 0$. The validity of this simple argumentation can be tested within AAT since the energy resolution of the AAT scheme is not limited by finite size effects. If we let $\eta \rightarrow 0$ states which are entirely concentrated on finite clusters do not contribute to the averaged density of states (remember the preliminary discussion), and only the continuous spectrum from extended band states survives. This spectrum indeed shows a gap around $\omega = 0$

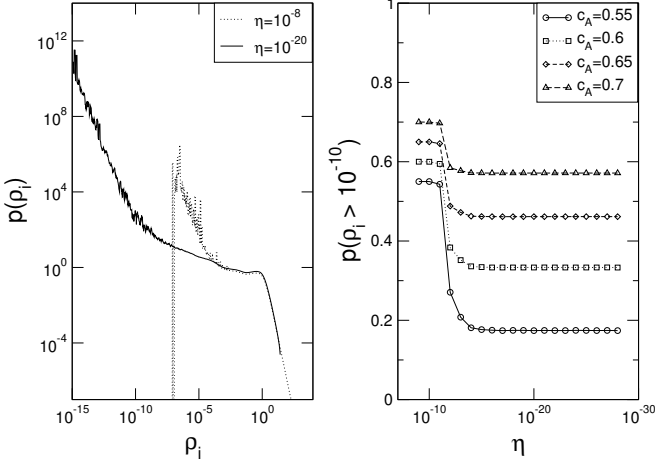


FIG. 8: Left panel: Distribution $p(\rho_i, \omega, \eta)$ for the percolation model at $\omega = 0.1$ and $c_A = 0.7$, for two values of regularization $\eta = 10^{-8}$ and $\eta = 10^{-20}$. Right panel: Integrated probability $p(\rho_i > \xi, \omega, \eta)$ in dependence on η , for $\omega = 0.1$, $c_A = 0.7, 0.6, 0.65, 0.55$, and one particular value $\xi = 10^{-10}$. For $c_A \lesssim 0.54$ no states exist at $\omega = 0.1$, and $p(\rho_i, \omega, \eta) = 0$.

for sufficiently small concentrations (cf. Fig. 7, bottom left). Lowering the concentration, gaps open at the energies corresponding to any finite cluster eigenstate. The first additional gaps open at $\omega = \pm t$ (Fig. 7, bottom right), corresponding to two site clusters, which have the second largest weight among all finite clusters. These gaps are filled by peaks from the dense spectrum of finite cluster states, thus are absent in the density of states for any finite energy resolution. The formation of gaps which is a kind of ‘level repulsion’ is a significant quantum feature with no counterpart in the classical model.

Besides the density of states the nature of states is important. For concentrations $c_A < p_c$, when only finite clusters exist, all states are localized and no electron transport is possible. The physics becomes more interesting for concentrations above p_c when a classical electron can traverse the system along the percolating cluster. But a quantum mechanical electron will scatter on all irregularities and is possibly localized. This raises the question of a quantum percolation threshold p_q above p_c .

Close to p_c states on the percolating cluster have only exponentially small weight. It is thus difficult to extract the information about those states from the background of finite cluster contributions. However, we can gain some information from the distribution of the local density of states, if c_A and η are varied. Again, if we let $\eta \rightarrow 0$, the energy resolution increases until finite cluster and percolating cluster states (that is, point vs. continuous spectrum) are separated from each other (cf. left panel of Fig. 8). For fixed energy ω and suitably large concentration c_A the distribution $p(\rho_i, \omega, \eta)$ has finite weight at finite ρ_i in the limit $\eta \rightarrow 0$ (cf. right panel of Fig. 8), which indicates that the states are extended. This weight can be quantified through the integrated proba-

bility $p(\rho_i > \xi, \omega, \eta) = \int_{\xi}^{\infty} p(\rho_i, \omega, \eta) d\rho_i$. The weight decreases with c_A , and abruptly drops to zero at a certain concentration (for $c_A \approx 0.54$ at $\omega = 0.1$). Then no states exist at ω , and $\rho_{\text{ave}}(\omega) = 0$. This behaviour has to be attributed to the fragmentation of the spectrum discussed before. At a given fixed energy ω a gap will open for concentrations sufficiently close to p_c . The gaps open at different concentrations for different energies, depending on the relative weight of a specific finite cluster. Between the gaps extended states can survive even for very small c_A , although all states are extremely damped and practically localized. Before a gap has opened, no states at ω exist. A localization transition from extended to localized states does not take place. The only transition occurs when the spectrum is fully fragmented, that is at $c_A = p_c$. We conclude that a quantum percolation threshold above the classical one does not exist. Let us remark that scattering in this situation is of a different type than for the Anderson model. The finite clusters attached to the percolating backbone do not act as coherent but incoherent scatterers. So states on the backbone will not be localized for small c_A (i.e. strong scattering), or even immediately localized, as in one dimension.

VIII. CONCLUSIONS

In this article we tried to demonstrate how the AAT scheme can be employed for thorough studies of disordered systems. We focused on three paradigmatic models, which show different physical aspects of real disordered solids. The localization transition in the Anderson model is an example for the subtle and complicated physical effects which can appear even in simple systems. The spatial correlations induced by quantum scattering are implicitly contained in the distribution of the local density of states which shows a characteristic behaviour close to the localization transition. The study of the dependence of this distribution on the η -regularization provided us with a precise localization criterion. With its help the phase diagram of the Anderson model has been calculated. AAT gives the complete picture known from a cubic lattice in three dimensions (the Bethe lattice does not hinder a proper description). We have thus demonstrated the central point of AAT: The *distribution* of the *local* density of states is an important quantity which fully reflects the complicated physics at the onset of localization. To stress the importance of distributions in the localization problem the AAT results have been compared to those from averaging theories which neglect all spatial correlations. As could be expected the CPA fails to detect localization at all, and ad hoc modifications of the CPA (i.e. TMT) give an inadequate description. A serious extension of CPA in terms of an $1/d$ -expansion has been recently derived and applied to the localization problem.²¹ Whether this extension can be successfully used for the purposes of our investigations has to be

clarified.

In contrast to the Anderson model with a smooth disorder distribution the binary alloy model shows rich features even in the averaged density of states which originate from the comparably stronger disorder fluctuations. Again the resulting physics is well described by the AAT approach. Even for the extreme limit of the binary alloy model, the percolation model, convincing results are easily obtained. The CPA, on the other hand, completely misses all interesting features, and fails in the full range of parameters.

Besides methodical questions new physical insight can be obtained using AAT. For instance the question whether gaps form in the percolation model could be definitely answered, and the possibility of a quantum percolation threshold above the classical one could be almost definitely ruled out. In contrast to the Anderson model the percolation model does not show an unambiguous phase transition in addition to the classical percolation transition. Even if it could be found the results obtained indicate that its relevance must be doubted. Similar questions become accessible within the AAT scheme even for *interacting* disordered systems. Then a proper though computationally not too demanding description of disorder physics becomes even more important. Surely interaction processes will be changed beyond renormalization of interaction parameters through the strong scattering processes in the binary alloy or the complicated quantum interference effect in the Anderson model. While investi-

gations guided by or based on the CPA must be suspected not to depict correct physical behaviour, an appropriate treatment can rely on the AAT scheme. A combination of AAT with a DMFT-treatment ('statistical DMFT')²² of electron-phonon-interaction has already been demonstrated to provide insight into the localization of a Holstein polaron.¹¹ A phenomenon like the formation of polaronic defect states, which should play an important role in 'real' polaronic materials, could be studied in detail. Such a cooperative phenomenon, where localized impurity states serve as germs for polaron formation, stresses the need for an appropriate treatment of disorder. Expectedly, averaging of spatial fluctuations removes all effects beyond the mean-field picture of diffusion from the theory. But remarkably enough, taking into account those fluctuations in even the simplest way—through distributions of a local quantity—is sufficient for a comprehensive description of disordered systems. Keeping this in mind the AAT scheme provides a kind of ultimate local approach to the disorder problem. As our results clearly show one should not try to get rid of the distributions it is based on. Honestly, two important points, critical behaviour at the localization transition and weak localization in 2d, cannot be addressed within the AAT approach. So AAT is surely no 'complete' theory but a convenient framework for investigations of disorder and localization, and if suitably extended, for interacting disordered systems.

¹ P. W. Anderson, Phys. Rev. **109**, 1492 (1958).
² A. MacKinnon and B. Kramer, Phys. Rev. Lett. **47**, 1546 (1981).
³ A. Georges, G. Kotliar, W. Krauth, and M. J. Rozenberg, Rev. Mod. Phys. **68**, 13 (1996).
⁴ R. J. Elliott, J. A. Krumhansl, and P. L. Leath, Rev. Mod. Phys. **46**, 465 (1974).
⁵ V. Dobrosavljević, A. A. Pastor, and B. K. Nikolić, Europhys. Lett. **62**, 76 (2003).
⁶ K. Byczuk, W. Hofstetter, and D. Vollhardt, Phys. Rev. B **69**, 045112 (2004).
⁷ M. Balzer and M. Potthoff (2004), cond-mat 0406266.
⁸ K. Byczuk, W. Hofstetter, and D. Vollhardt (2004), cond-mat 0403765.
⁹ M. Jarrell and H. R. Krishnamurthy, Phys. Rev. B **63**, 125102 (2001).
¹⁰ R. Abou-Chakra, P. W. Anderson, and D. J. Thouless, J. Phys. C **6**, 1734 (1973).
¹¹ F. X. Bronold, A. Alvermann, and H. Fehske, Phil. Mag. **84**, 673 (2004).
¹² E. N. Economou, *Green's Functions in Quantum Physics* (Springer-Verlag, Berlin, 1983).

¹³ A. D. Mirlin and Y. V. Fyodorov, Phys. Rev. Lett. **72**, 526 (1994).
¹⁴ K. B. Efetov and O. Viehweger, Phys. Rev. B **45**, 11546 (1992).
¹⁵ K. B. Efetov and V. N. Prigodin, Phys. Rev. Lett. **70**, 1315 (1993).
¹⁶ B. Kramer and A. MacKinnon, Rep. Prog. Phys. **56**, 1469 (1993).
¹⁷ G. Schubert, A. Weiße, G. Wellein, and H. Fehske, in *High Performance Computing in Science and Engineering* (Springer-Verlag Berlin Heidelberg, 2005).
¹⁸ S. Kirkpatrick and T. P. Eggarter, Phys. Rev. B **72**, 3598 (1972).
¹⁹ C. M. Soukoulis, Q. Li, and G. S. Grest, Phys. Rev. B **45**, 7724 (1992).
²⁰ I. V. Plyushchay, R. A. Römer, and M. Schreiber, Phys. Rev. B **68**, 064201 (2003).
²¹ V. Janiš and J. Kolorenč (2004), cond-mat 0402471.
²² V. Dobrosavljević and G. Kotliar, Phil. Trans. R. Soc. Lond. A **356**, 57 (1998).